



Deposited via The University of York.

White Rose Research Online URL for this paper:

<https://eprints.whiterose.ac.uk/id/eprint/188842/>

Version: Published Version

---

**Article:**

Ivatt, Peter David, Evans, Mathew John and Lewis, Alastair (2022) Suppression of surface ozone by an aerosol-inhibited photochemical ozone regime. *Nature Geoscience*. pp. 536-540. ISSN: 1752-0908

<https://doi.org/10.1038/s41561-022-00972-9>

---

**Reuse**

This article is distributed under the terms of the Creative Commons Attribution (CC BY) licence. This licence allows you to distribute, remix, tweak, and build upon the work, even commercially, as long as you credit the authors for the original work. More information and the full terms of the licence here:

<https://creativecommons.org/licenses/>

**Takedown**

If you consider content in White Rose Research Online to be in breach of UK law, please notify us by emailing [eprints@whiterose.ac.uk](mailto:eprints@whiterose.ac.uk) including the URL of the record and the reason for the withdrawal request.



OPEN

# Suppression of surface ozone by an aerosol-inhibited photochemical ozone regime

Peter D. Ivatt<sup>1,2</sup>, Mathew J. Evans <sup>1,2</sup>✉ and Alastair C. Lewis <sup>1,2</sup>

**Atmospheric ozone (O<sub>3</sub>) is a pollutant produced through chemical chain reactions where volatile organic compounds (VOCs), carbon monoxide and methane are oxidized in the presence of oxides of nitrogen (NO<sub>x</sub>). For decades, the controlling chain termination step has been used to separate regions into either 'NO<sub>x</sub> limited' (peroxyl-radical self-reactions dominate) or 'VOC limited' (hydroxyl radical (OH) + nitrogen dioxide (NO<sub>2</sub>) reaction dominates). The controlling regime would then guide policies for reducing emissions and so O<sub>3</sub> concentrations. Using a chemical transport model, we show that a third 'aerosol inhibited' regime exists, where reactive uptake of hydroperoxyl radicals (HO<sub>2</sub>) onto aerosol particles dominates. In 1970, 2% of the Northern Hemisphere population lived in an aerosol-inhibited regime, but by 2014 this had increased to 21%; 60% more than lived in a VOC-limited regime. Aerosol-inhibited chemistry suppressed surface O<sub>3</sub> concentrations in North America and Europe in the 1970s and is currently suppressing surface O<sub>3</sub> over Asia. This third photochemical O<sub>3</sub> regime leads to potential trade-off tensions between reducing particle pollution in Asia (a key current health policy and priority) and increasing surface O<sub>3</sub>, should O<sub>3</sub> precursors emissions not be reduced in tandem.**

Ozone (O<sub>3</sub>) has well-documented detrimental impacts on human and ecosystem health, and in the mid to upper free troposphere is a greenhouse gas<sup>1,2</sup>. Since the mid-twentieth century, it has been known that O<sub>3</sub> is formed through complex radical chain-reaction chemistry involving the oxidation of volatile organic compounds (VOCs) in the presence of oxides of nitrogen (NO<sub>x</sub>) (ref. <sup>3</sup>). The chain reaction is initiated through the photolysis of photo-labile compounds such as O<sub>3</sub>, CH<sub>2</sub>O and HONO, propagated through the interconversion of peroxy (HO<sub>2</sub> and RO<sub>2</sub>) and hydroxyl (OH) radicals and terminated either through the self-reaction of peroxy radicals to form longer-lived species (such as peroxides) or from the reaction of a hydroxyl radical with nitrogen dioxide (NO<sub>2</sub>) to form nitric acid (HNO<sub>3</sub>)<sup>4,5</sup>. From the perspective of reducing O<sub>3</sub> pollution, the dominant termination step is often used to identify whether reductions in the emissions of NO<sub>x</sub> or VOCs should be preferentially employed<sup>6</sup>. If peroxy-radical self-reactions dominate (known as the 'NO<sub>x</sub> limited' regime), reductions in NO<sub>x</sub> emissions are most beneficial, whereas if the NO<sub>2</sub> + OH reaction dominates (known as the 'VOC limited' regime) reductions in organic emissions are most effective. The existence of these two well-defined O<sub>3</sub> production regimes has been used to guide national-, regional- and city-level air-quality policy choices for many decades<sup>3</sup>.

Since the development of the NO<sub>x</sub>- versus VOC-limited model, understanding of atmospheric chemistry has advanced, with increased understanding of VOC chemistry<sup>7</sup>, aerosols<sup>8</sup>, halogens<sup>9</sup> and so on. In this study, we use a chemistry transport model with an advanced representation of atmospheric chemistry (GEOS-Chem<sup>10</sup>) to diagnose the balance of termination steps. Notably, the model includes the uptake of HO<sub>2</sub> onto aerosol surfaces, which has been identified as an important process for chain termination over the past decades<sup>8,11–15</sup>. We compare the rate of radical termination by peroxy-radical self-reactions, the OH + NO<sub>2</sub> reaction and the uptake of HO<sub>2</sub> onto aerosol in July for the Northern Hemisphere in the pre-industrial era (1750), 1970 and 2014 (Methods).

Concentrations of key components calculated by the model are shown in Supplementary Figs. 1–6.

## Chain termination

Figure 1 shows the surface distribution of the relative chemical fluxes of these termination steps for July 1750, 1970 and 2014 (enlargements over North America, Europe and Asia are in Supplementary Figs. 8–10).

In the pre-industrial era (1750), peroxy-radical self-reactions (green) dominate. Biomass burning (forest fires) in Russia and Canada show termination by the uptake of HO<sub>2</sub> onto aerosol (blue), whereas fires over Kazakhstan show termination by OH + NO<sub>2</sub> (red) (Extended Data Fig. 1 shows a simulation with biomass burning switched off). This reflects the differing balance of NO<sub>x</sub> relative to particulates emitted by different fires<sup>16</sup>. Desert dust makes only a limited contribution to the aerosol surface area, leading to some increased contribution of HO<sub>2</sub> uptake over Mauritania, Oman and Iran, but overall the impact is minor (Extended Data Fig. 1 shows a simulation with no desert dust emissions). Some HO<sub>2</sub> uptake by sea salt occurs over the northern Atlantic/Pacific and over the Arabian sea (Extended Data Fig. 1 shows a simulation with no sea-salt emissions).

In 1970, industrial and transport emissions over North America, Europe and Japan<sup>17</sup> have a profound impact on the radical termination processes. Many of the cities in North America, Europe and Japan are red, indicating NO<sub>2</sub> + OH as the dominant termination step. However, over Europe, large regions of the North Sea and eastern Germany are magenta (balance between OH + NO<sub>2</sub> and aerosol uptake), with much of eastern Europe being cyan (balance between peroxy-radical self-reaction and aerosol uptake). Over North America, West Coast cities (Los Angeles, San Francisco and Seattle) show NO<sub>2</sub> + OH domination, while cities around the Great Lakes and those on the East Coast show large fractions of the radical termination being due to HO<sub>2</sub> uptake (magenta, cyan), reflecting the different industrial and transport sources in these regions. Most of Japan is red or yellow,

<sup>1</sup>Department of Chemistry, University of York, York, UK. <sup>2</sup>National Centre for Atmospheric Science, University of York, York, UK.

✉e-mail: [mat.evans@york.ac.uk](mailto:mat.evans@york.ac.uk)

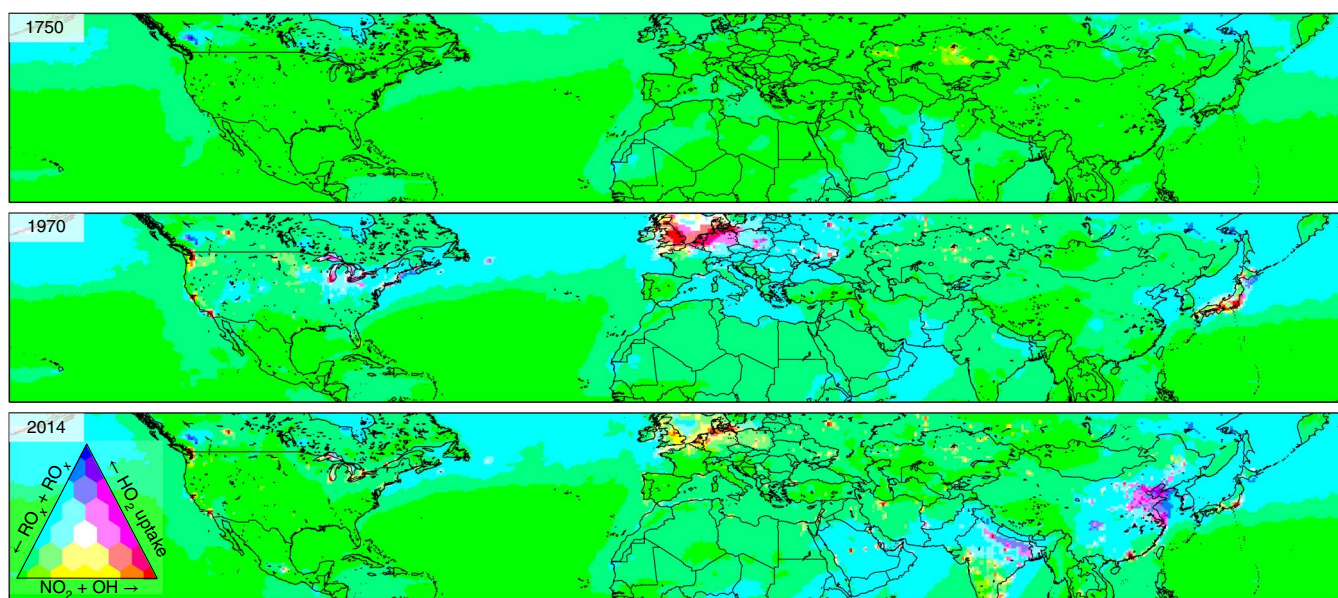


**Fig. 1 | Map of the fractional contribution of each radical loss pathway for the years 1750, 1950 and 2014.** Mean simulated July solar noon-time fraction of radical termination at the surface that occurs through  $\text{OH} + \text{NO}_2$  (red), peroxy-radical self-reactions (green) and aerosol uptake of  $\text{HO}_2$  (blue) for 1750, 1970 and 2014. Enlargements of North America, Europe and Asia are shown in the Supplementary Information.

showing limited impact of  $\text{HO}_2$  uptake. In 1970, China and India remain dominated by peroxy-radical self-reaction, but there is some increased uptake of  $\text{HO}_2$  by aerosols over populated regions relative to the pre-industrial era. Extensive areas of the oceans are cyan, indicating large  $\text{HO}_2$  uptake. Some of this is driven by sea salt (Extended Data Fig. 1), but some is driven by shipping emissions (see Extended Data Fig. 2 without shipping emissions) and some by outflow of aerosol from industrial regions.

By 2014, the balance has changed as North America, Europe and Japan implemented policies to substantially reduce emissions of  $\text{NO}_x$ , VOCs, primary aerosols and aerosol precursors<sup>17</sup>. The relative importance of both  $\text{OH} + \text{NO}_2$  and  $\text{HO}_2$  uptake onto aerosols for termination has reduced, reflecting these emissions reductions. Over Asia, however, emissions have increased due to population growth and industrialization, leading to increases in  $\text{NO}_x$  and PM concentrations. Large regions are now coloured magenta (balanced  $\text{HO}_2$  uptake and  $\text{OH} + \text{NO}_2$ ) or blue (dominated by  $\text{HO}_2$  uptake).

This behaviour is seen predominantly within the boundary layer (Extended Data Fig. 3). In regions with more active mixing between the surface and the mid-troposphere, uptake onto aerosols can remain regionally important at 800 hPa, and  $\text{NO}_2 + \text{OH}$  can be important over cities. In general, the importance of these regimes decreases through the atmosphere so that at 500 hPa, the atmosphere is dominated by peroxy-radical self-reactions. At higher altitudes, lightning  $\text{NO}_x$  can lead to an increase in the importance of  $\text{NO}_2 + \text{OH}$  as a termination process.

### Photochemical regimes

Figure 2 splits the domain based on the local largest termination step (enlarged versions for North America, Europe and Asia are in Supplementary Figs. 11–13). At a global scale, most locations are in an  $\text{NO}_x$ -limited regime (green), with some cities in a VOC-limited (red) regime. However, for large regions, the uptake of  $\text{HO}_2$  onto aerosol (blue) is the largest termination reaction, and thus they do not fall into either of the two classically applied policy-control regimes. We call this third regime ‘aerosol inhibited’ as the presence of aerosols inhibits the formation of  $\text{O}_3$  on short photochemical timescales. Area- and population-weighted

fractions over differing regions for the three regimes are given in Supplementary Tables 1 and 2.

As with the radical loss plot (Fig. 1), in 1750 the world was dominated by radical self-reactions, and so, except for forest-fire locations, the world was entirely  $\text{NO}_x$  limited. In the 1970s, the large North American cities, northern Europe and southern Japan had become VOC limited. Although not recognized at the time, aerosol-inhibited regimes existed in regions downwind of these VOC-limited environments (eastern seaboard of the United States, Poland, downwind of Japan) and in some remote locations impacted by desert dust and shipping. In 1970, around 30% of the populations of Europe and North America and 71% of the population of Japan lived in VOC-limited regions, but only a small portion (<10%) lived in an aerosol-inhibited regime. Negligible fractions lived in that regime in the rest of the Northern Hemisphere.

By 2014, the success of air-quality strategies meant that aerosol-inhibited regimes over Europe and North America had mostly disappeared, leaving behind some relatively polluted city regions as VOC limited, but with most people living in  $\text{NO}_x$ -limited regions (80% in Europe and North America, 66% in Japan). However, industrialization in Asia moved many cities to be VOC limited (19% in China and 11% in India), but much larger populations in those regions live in aerosol-inhibited regions (36% and 39%, respectively), notably, in the Indo-Gangetic Plain and eastern China. The aerosol-inhibited regime plays a more important role in Asia in 2014 than it did in Europe and North America in 1970.

Understanding of the chemistry in this new third photochemical regime is still poor. The reactive uptake coefficient for  $\text{HO}_2$  on aerosol ( $\gamma_{\text{HO}_2}$ ) can vary by orders of magnitude depending on relative humidity, aerosol composition and the concentration of transition metals<sup>12,18–21</sup>. The work here assumes a uniform  $\gamma_{\text{HO}_2}$  of 0.2, consistent with previous modelling work<sup>13</sup>. Simulations run with a  $\gamma_{\text{HO}_2}$  of 0.1 still lead to regions in the aerosol-inhibited regime (Extended Data Fig. 4), but the fraction of the population living in this regime reduces (9% of China and 5% of India). A reduction in the  $\gamma_{\text{HO}_2}$  to 0.05 results in some areas still being within the regime, but these are now restricted to coastal Chinese regions. A  $\gamma_{\text{HO}_2}$  of less than 0.05 as suggested by some early studies<sup>20</sup> would probably

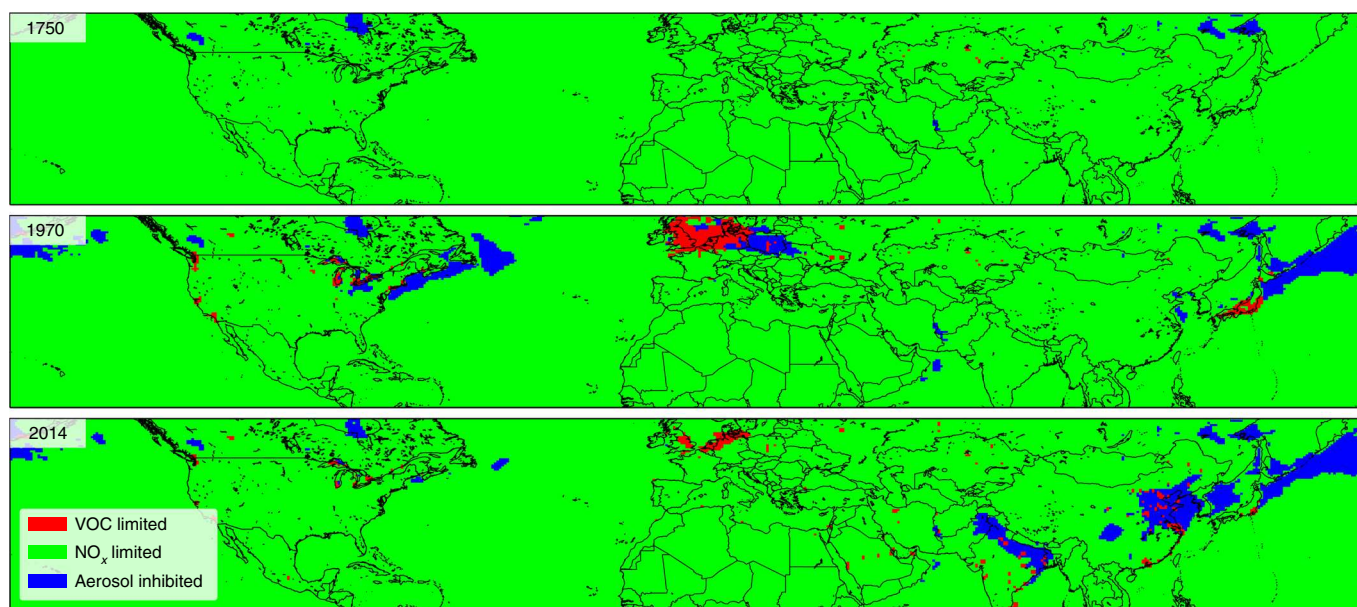


**Fig. 2 | Map of the photochemical ozone-control regime for the years 1750, 1950 and 2014.** Mean simulated July solar noon-time photochemical ozone-control regime for 1750, 1970 and 2014. Enlargements of North America, Europe and Asia are shown in the Supplementary Information.

result in very few locations being in the aerosol-inhibited regime. Thus with our model, this new photochemical regime exists for  $\gamma_{\text{HO}_2}$  greater than 0.05 and is probably important for values greater than 0.1. Field observations of radicals in the aerosol-inhibited regions are rare. Observations and box modelling made in central Beijing<sup>22</sup> show a VOC-limited regime consistent with the modelling here, with similar conclusions for central New Delhi<sup>23</sup>. Observations from a more remote site in the North China Plain<sup>24</sup> suggest an  $\text{NO}_x$ -limited regime, whereas the modelling here would suggest an aerosol-limited one for that location. Reducing the  $\gamma_{\text{HO}_2}$  to 0.1 would give a consistent response here. Another area little explored is the ability to simulate aerosol surface-area density in models (Supplementary Fig. 7). Mass of particulate matter less than  $2.5\ \mu\text{m}$  in diameter ( $\text{PM}_{2.5}$ ) is often evaluated in models since it is the primary health metric and more readily observable<sup>25</sup>, and sometimes aerosol number density is evaluated because of its important role in light scattering and cloud–aerosol interaction<sup>26</sup>, but systematic evaluations of modelled aerosol surface area are rare.

### Impact on $\text{O}_3$

The additional radical sink offered by the uptake of  $\text{HO}_2$  onto aerosol has a profound effect on regional  $\text{O}_3$  concentrations. Figure 3 shows the impact on  $\text{O}_3$  concentrations of switching off the uptake of  $\text{HO}_2$  onto aerosol ( $\gamma_{\text{HO}_2} = 0$ ). In the pre-industrial 1750 simulation, the reactive uptake of  $\text{HO}_2$  onto aerosols has a small impact on  $\text{O}_3$  concentrations (<2%). The only places where increases in  $\text{O}_3$  can be seen is over the biomass-burning regions of Canada and Russia.

In 1970, industrialized regions of North America, Europe and Japan show larger impacts. Substantial increases in  $\text{O}_3$  concentrations are seen in northern Germany (28%), Tokyo (18%) and the American Great Lakes (20%). Los Angeles displays the largest impact, resulting in a 35% increase in  $\text{O}_3$  concentrations when  $\text{HO}_2$  uptake is switched off. The  $\text{O}_3$  changes over India and China in 1970 were less than 5%. Thus, for many parts of North America, Europe and Japan in the 1970s, particulate pollution enhanced the uptake of  $\text{HO}_2$  onto aerosols and reduced  $\text{O}_3$  pollution.

By 2014,  $\text{O}_3$  sensitivity to  $\text{HO}_2$  uptake had reduced in Europe, North America and Japan as policy interventions had reduced particulate-matter concentrations. Removing  $\text{HO}_2$  uptake in those simulations leads to less than a 5% increase in  $\text{O}_3$  concentrations.

Over China, however, removing the uptake of  $\text{HO}_2$  onto aerosol increases  $\text{O}_3$  concentrations in the North China plain by between 20% and 30%. Even higher values (>35%) can be seen over the Bohai and Yellow seas. An additional hot spot can be seen inland over Chengdu. The Indo-Gangetic Plain has some of the highest observed sensitivity globally, with  $\text{O}_3$  increases of greater than 30%. Uptake of  $\text{HO}_2$  within the model thus has a large influence on surface  $\text{O}_3$  concentration, notably in present-day China and India.

### Discussion

Although we have identified regions that are aerosol inhibited from a fast photochemical perspective, aerosols can have an impact on  $\text{O}_3$  production more widely through a number of processes: other heterogeneous reactions<sup>27,28</sup>, changes to photolysis rates<sup>29</sup> and changes to the boundary layer<sup>30</sup>. Thus, although the area might be aerosol inhibited from a radical perspective, the overall impact of a change of aerosol concentration may be more complicated.

Future work is necessary to better evaluate modelled aerosol surface area and to create a robust parameterization for  $\gamma_{\text{HO}_2}$ . It would also be useful to have observational data in regions outside of large cities but subject to high particulate pollution as these are the areas influenced by the new regime. The existence, however, of a third aerosol-inhibited photochemical ozone regime, which currently covers large regions and populations in China and India, highlights the complexity of implementing policies to improve air quality. Strategies that focus on reducing particulate matter alone create a trade-off with increases in surface ozone, a phenomenon observed in China<sup>13,31</sup>. A simulation (Methods) over India, where the 2014 emissions of anthropogenic particulate precursors ( $\text{SO}_2$ , black carbon, organic carbon and dust) and biomass burning are halved (representing an aggressive air-quality intervention) leads to reduced particle surface-area densities (Extended Data Fig. 5) and increased  $\text{O}_3$  concentrations (Extended Data Fig. 6). To counter this adverse outcome, policy development must account for the aerosol-inhibited regime and include contemporaneous reductions in other anthropogenic emissions. Figure 4 shows the fractional reductions in anthropogenic  $\text{NO}_x$  emissions that are necessary to mitigate the additional  $\text{O}_3$  that would form from this aerosol emissions reduction. For a large part of the Indo-Gangetic plain, large (~40%) parallel reductions in  $\text{NO}_x$  emissions would be needed to

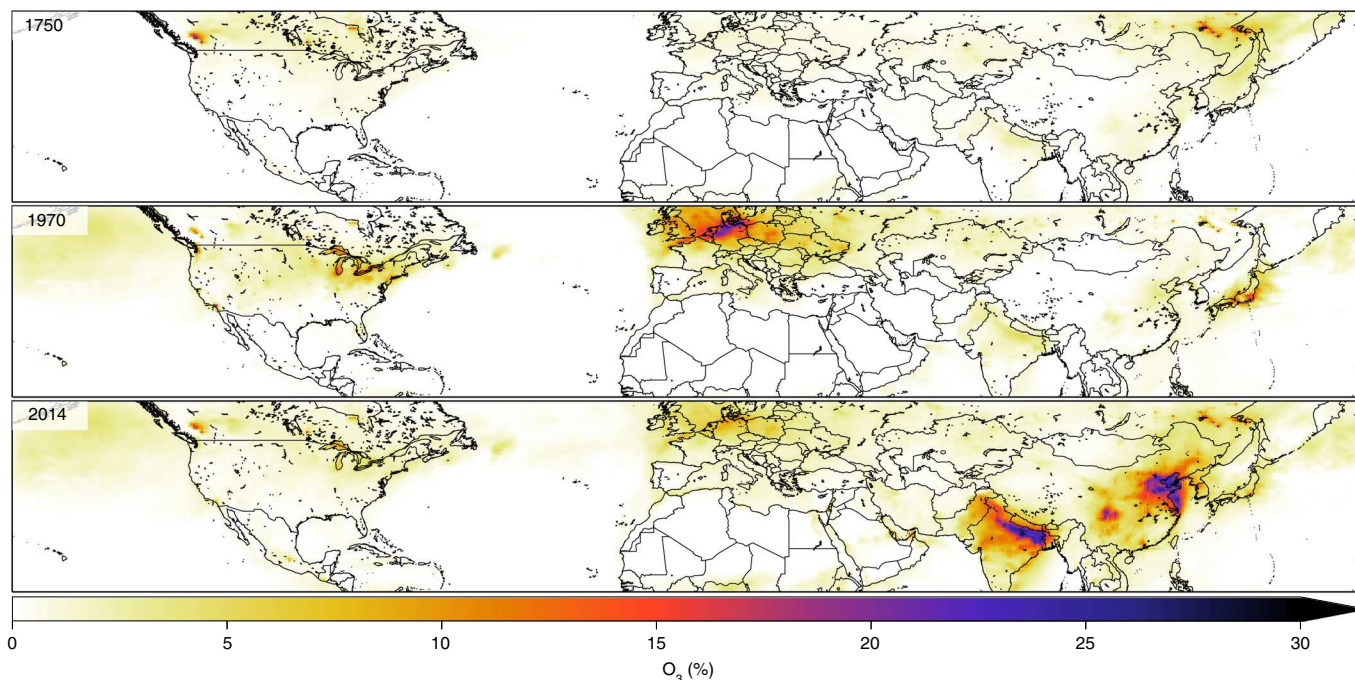


**Fig. 3 | Map of the percentage increase in ozone concentration when uptake of HO<sub>2</sub> is switched off for 1750, 1970 and 2014.** Percentage increase in monthly mean solar 15:00 LT O<sub>3</sub> concentration for July when heterogeneous uptake of HO<sub>2</sub> on aerosols is switched off for 1750, 1970 and 2014.

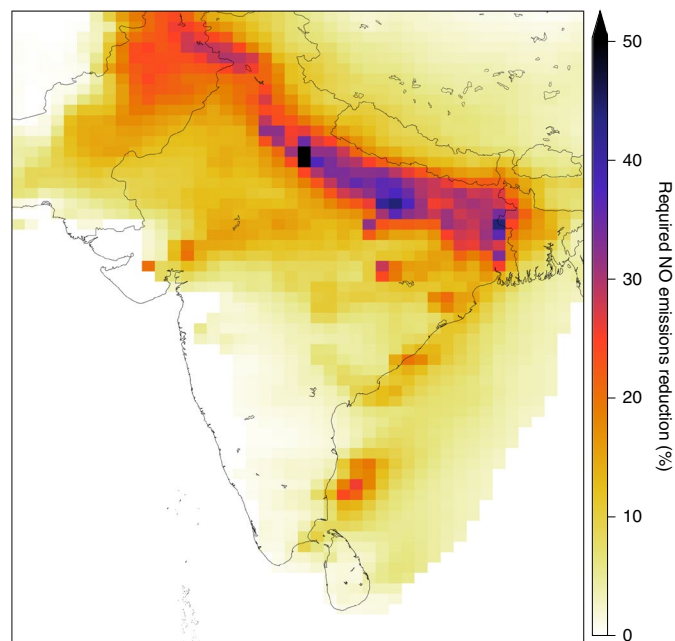


**Fig. 4 | Map of fractional NO<sub>x</sub> emissions decrease required to offset a 50% reduction in aerosol emissions.** Fractional decrease in 2014 NO<sub>x</sub> emissions that is necessary to offset the increase in surface, monthly mean and solar 15:00 LT O<sub>3</sub> caused by a 50% reduction in emissions of aerosol precursors (anthropogenic SO<sub>2</sub>, black carbon, organic carbon, dust and all biomass-burning emissions).

stop O<sub>3</sub> concentrations from increasing. Although the direct health gains of reducing particulate-matter emissions will probably outweigh the disbenefits on health from increasing O<sub>3</sub> concentrations, there would probably be additional negative impacts on ecosystems,

crop yield reductions and regional climate warming that would arise if aerosol-inhibition effects were not managed.

#### Online content

Any methods, additional references, Nature Research reporting summaries, source data, extended data, supplementary information, acknowledgements, peer review information; details of author contributions and competing interests; and statements of data and code availability are available at <https://doi.org/10.1038/s41561-022-00972-9>.

Received: 17 August 2021; Accepted: 20 May 2022;

Published online: 07 July 2022

#### References

1. Fowler, D. et al. *Ground-Level Ozone in the 21st Century: Future Trends, Impacts and Policy Implications* (The Royal Society, 2008).
2. IPCC *Climate Change 2014: Synthesis Report* (eds Core Writing Team, Pachauri, R. K. & Meyer, L. A.) (IPCC, 2014).
3. Council, N. R. *Rethinking the Ozone Problem in Urban and Regional Air Pollution* (National Academies Press, 1991).
4. Sillman, S. The relation between ozone, NO<sub>x</sub> and hydrocarbons in urban and polluted rural environments. *Atmos. Environ.* **33**, 1821–1845 (1999).
5. Thornton, J. A. et al. Ozone production rates as a function of NO<sub>x</sub> abundances and HO<sub>x</sub> production rates in the Nashville urban plume. *J. Geophys. Res. Atmos.* **107**, 4146 (2002).
6. Sillman, S. & He, D. Y. Some theoretical results concerning O<sub>3</sub>–NO<sub>x</sub>–VOC chemistry and NO<sub>x</sub>–VOC indicators. *J. Geophys. Res. Atmos.* **107**, 4659 (2002).
7. Lelieveld, J. et al. Atmospheric oxidation capacity sustained by a tropical forest. *Nature* **452**, 737–740 (2008).
8. Jacob, D. J. Heterogeneous chemistry and tropospheric ozone. *Atmos. Environ.* **34**, 2131–2159 (2000).
9. Read, K. A. et al. Extensive halogen-mediated ozone destruction over the tropical Atlantic Ocean. *Nature* **453**, 1232–1235 (2008).
10. Bey, I. et al. Global modeling of tropospheric chemistry with assimilated meteorology: model description and evaluation. *J. Geophys. Res. Atmos.* **106**, 23073–23095 (2001).
11. Martin, R. V., Jacob, D. J., Yantosca, R. M., Chin, M. & Ginoux, P. Global and regional decreases in tropospheric oxidants from photochemical effects of aerosols. *J. Geophys. Res. Atmos.* **108**, 4097 (2003).

12. Song, H. et al. Influence of aerosol copper on HO<sub>2</sub> uptake: a novel parameterized equation. *Atmos. Chem. Phys.* **20**, 15835–15850 (2020).
13. Li, K. et al. A two-pollutant strategy for improving ozone and particulate air quality in China. *Nat. Geosci.* **12**, 906–910 (2019).
14. Sakamoto, Y. et al. Relative and absolute sensitivity analysis on ozone production in Tsukuba, a city in Japan. *Environ. Sci. Technol.* **53**, 13629–13635 (2019).
15. Song, H. et al. Reduced aerosol uptake of hydroperoxyl radical may increase the sensitivity of ozone production to volatile organic compounds. *Environ. Sci. Technol. Lett.* **9**, 22–29 (2022).
16. Giglio, L., Randerson, J. T. & van der Werf, G. R. Analysis of daily, monthly, and annual burned area using the fourth-generation global fire emissions database (GFED4). *J. Geophys. Res. Biogeosci.* **118**, 317–328 (2013).
17. Hoesly, R. M. et al. Historical (1750–2014) anthropogenic emissions of reactive gases and aerosols from the Community Emissions Data System (CEDS). *Geosci. Model Dev.* **11**, 369–408 (2018).
18. Cooper, P. L. & Abbatt, J. P. D. Heterogeneous interactions of OH and HO<sub>2</sub> radicals with surfaces characteristic of atmospheric particulate matter. *J. Phys. Chem.* **100**, 2249–2254 (1996).
19. Thornton, J. A., Jaegle, L. & McNeill, V. F. Assessing known pathways for HO<sub>2</sub> loss in aqueous atmospheric aerosols: regional and global impacts on tropospheric oxidants. *J. Geophys. Res., Atmos.* **113**, D05303 (2008).
20. Macintyre, H. L. & Evans, M. J. Parameterisation and impact of aerosol uptake of HO<sub>2</sub> on a global tropospheric model. *Atmos. Chem. Phys.* **11**, 10965–10974 (2011).
21. Zhou, J. et al. Kinetics and impacting factors of HO<sub>2</sub> uptake onto submicron atmospheric aerosols during the 2019 air quality study (aquas) in Yokohama, Japan. *Atmos. Chem. Phys.* **21**, 12243–12260 (2021).
22. Whalley, L. K. et al. Evaluating the sensitivity of radical chemistry and ozone formation to ambient VOCs and NO<sub>x</sub> in Beijing. *Atmos. Chem. Phys.* **21**, 2125–2147 (2021).
23. Nelson, B. S. et al. In situ ozone production is highly sensitive to volatile organic compounds in Delhi, India. *Atmos. Chem. Phys.* **21**, 13609–13630 (2021).
24. Tan, Z. F. et al. No evidence for a significant impact of heterogeneous chemistry on radical concentrations in the North China plain in summer 2014. *Environ. Sci. Technol.* **54**, 5973–5979 (2020).
25. Mortier, A. et al. Evaluation of climate model aerosol trends with ground-based observations over the last 2 decades—an AeroCom and CMIP6 analysis. *Atmos. Chem. Phys.* **20**, 13355–13378 (2020).
26. Fanourgakis, G. S. et al. Evaluation of global simulations of aerosol particle and cloud condensation nuclei number, with implications for cloud droplet formation. *Atmos. Chem. Phys.* **19**, 8591–8617 (2019).
27. Dentener, F. & Crutzen, P. J. Reaction of H<sub>2</sub>O<sub>2</sub> on tropospheric aerosols: impact on the global distributions of NO<sub>x</sub>, O<sub>3</sub>, and OH. *J. Geophys. Res., Atmos.* **98**, 7149–7163 (1993).
28. Kleffmann, J., Becker, K. & Wiesen, P. Heterogeneous NO<sub>2</sub> conversion processes on acid surfaces: possible atmospheric implications. *Atmos. Environ.* **32**, 2721–2729 (1998).
29. He, S. & Carmichael, G. R. Sensitivity of photolysis rates and ozone production in the troposphere to aerosol properties. *J. Geophys. Res., Atmos.* **104**, 26307–26324 (1999).
30. Jacobson, M. Z. Studying the effects of aerosols on vertical photolysis rate coefficient and temperature profiles over an urban airshed. *J. Geophys. Res., Atmos.* **103**, 10593–10604 (1998).
31. Ma, Z. et al. Significant increase of surface ozone at a rural site, north of eastern China. *Atmos. Chem. Phys.* **16**, 3969–3977 (2016).

**Publisher's note** Springer Nature remains neutral with regard to jurisdictional claims in published maps and institutional affiliations.



**Open Access** This article is licensed under a Creative Commons Attribution 4.0 International License, which permits use, sharing, adaptation, distribution and reproduction in any medium or format, as long as you give appropriate credit to the original author(s) and the source, provide a link to the Creative Commons license, and indicate if changes were made. The images or other third party material in this article are included in the article's Creative Commons license, unless indicated otherwise in a credit line to the material. If material is not included in the article's Creative Commons license and your intended use is not permitted by statutory regulation or exceeds the permitted use, you will need to obtain permission directly from the copyright holder. To view a copy of this license, visit <http://creativecommons.org/licenses/by/4.0/>.

© The Author(s) 2022

## Methods

**Model.** GEOS-Chem<sup>10</sup> version 12.8 (<http://www.geos-chem.org>) was run in the tropchem configuration, which consists of 536 gas-phase, 76 heterogeneous and 133 photolytic reactions. Within the stratosphere, a linearized chemistry was used<sup>32</sup>.

The same meteorology was used for each simulation, but anthropogenic emissions were varied on the basis of the Community Emissions Data System<sup>17</sup> emissions for 1750, 1970 and 2014 (the last available year). For each emissions year, the model was run globally at 4° × 5° for two years with the first year considered as spin-up. Boundary conditions and initial conditions were generated from the second year of simulation. These were then used in a one-month (1 June to 31 June) 1.00° × 1.25° nested simulation over a domain of 10° to 60° N latitude and 170° W to 170° E longitude to provide initial conditions for a final 0.500° × 0.625° simulation (1 July to 31s July) run over the same domain. The concentrations of all species within the chemistry scheme were archived each model time step from the high-resolution simulation, and these were then used to calculate chemical fluxes.

The GEOS-FP (forward processing) meteorological fields from the NASA Global Modelling and Assimilation Office (<https://gmao.gsfc.nasa.gov/>) drove model transport. All simulations used 47 vertical levels extending from the surface to approximately 80 km in altitude.

Other emissions were kept the same in all simulations: the MEGAN<sup>33</sup> inventory provided the biogenic emissions, GFED<sup>46</sup> provided the biomass-burning emissions and DEAD<sup>34</sup> provided the dust emissions.

**Loss rates.** Chain-reaction termination rates were calculated offline from the archived species concentrations, physical parameters (temperature, pressure and humidity), aerosol parameters (component surface areas and radii) and the model rate constants.

We do not count the production of radical products in the peroxy-radical self-reaction as termination steps but do assume that non-radical products are long lived on the timescale of the calculation and so offer a chain termination step.

The heterogeneous radical loss rate of HO<sub>2</sub> was calculated by iterating over the radius and surface area of each type of aerosol (organic carbon, black carbon, dust, sea salt, nitrate-sulfate-ammonium and secondary organic aerosol). These parameters were used in conjunction with temperature and air density to calculate the first-order HO<sub>2</sub> loss rate.

We calculate the flux through each chemical termination route at local solar noon for each grid box for each day of July and sum. We divide the individual monthly sums for each termination process by the total of the three termination processes over the month to derive the fractions shown.

Following ref. <sup>6</sup>, we define a grid box's O<sub>3</sub> control regime by the largest of the three termination route.

**HO<sub>2</sub> uptake coefficient.** We have used a default HO<sub>2</sub> reactive uptake coefficient ( $\gamma_{\text{HO}_2}$ ) of 0.2 (ref. <sup>9</sup>). Laboratory studies using pure synthetic aerosol have found relatively low ( $\gamma_{\text{HO}_2} < 0.2$ ) values of uptake coefficients<sup>18,35–37</sup>; however, studies on real-world aerosol have found greater coefficients ranging from 0.08 to 0.40 (refs. <sup>21,38,39</sup>). It is likely that minor components of the aerosol such as transition metals may play an important role in this. Some evidence suggests copper appears to greatly enhance the uptake coefficients<sup>40–42</sup>, and this has been shown to be present in Asian aerosol<sup>43–45</sup>.

We run simulations where the  $\gamma_{\text{HO}_2}$  is reduced to 0.1, 0.05 and 0.00 and show results in Extended Data Fig. 4. We treat H<sub>2</sub>O as the sole product formed during the heterogeneous uptake of HO<sub>2</sub><sup>46</sup>, but our conclusions do not change if we assume production of H<sub>2</sub>O<sub>2</sub>.

The use of a single value of  $\gamma_{\text{HO}_2}$  is unlikely to be realistic. However, current parameterizations do not reproduce the observed temporal variability in  $\gamma_{\text{HO}_2}$  (ref. <sup>21</sup>). Further study will be needed to provide an appropriate parameterization for  $\gamma_{\text{HO}_2}$ . How the value of  $\gamma_{\text{HO}_2}$  varies with the changing concentration of NO<sub>x</sub> and radicals is likely to play an important role in determining the importance of HO<sub>2</sub> uptake for controlling O<sub>3</sub> concentrations.

**Indian particulate emissions reductions.** Over a more limited Indian domain (3° to 36° N latitude and 63° to 94° E longitude), we repeat the July 2014 simulation at 0.25° by 0.3125°. We then half the 2014 emissions of anthropogenic particulate precursors (SO<sub>2</sub>, black carbon, organic carbon and anthropogenic dust) and all biomass-burning emissions to simulate an aggressive local effort to reduce particulate-matter pollution. This reduces particulate surface-area densities substantially (Extended Data Fig. 5) and leads to increased O<sub>3</sub> concentrations (Extended Data Fig. 6). With the reduced particulate-matter emissions, we then run five simulations reducing anthropogenic NO<sub>x</sub> emissions by 10%, 20%, 30%, 40% and 50%. For each surface model grid box, we fit a third-order polynomial through a graph of monthly mean 15:00 LT O<sub>3</sub> concentration against the percentage NO<sub>x</sub> reduction and identify when the value of NO<sub>x</sub> emissions reduction gives the same mean O<sub>3</sub> concentration as in the simulation without any reduction in particulate-matter emissions. This value of NO<sub>x</sub> reduction is then plotted for each grid box as in Fig. 4.

## Data availability

All data used to produce this paper are available at <https://doi.org/10.5285/406f88e14f34177934b1dbd0be6aac7>.

## Code availability

The GEOS-Chem model is available from <https://github.com/geoschem/geos-chem>. Code used to draw up the figures in the paper are deposited alongside the data.

## References

- Eastham, S. D., Weisenstein, D. K. & Barrett, S. R. H. Development and evaluation of the unified tropospheric-stratospheric chemistry extension (UCX) for the global chemistry-transport model GEOS-Chem. *Atmos. Environ.* **89**, 52–63 (2014).
- Guenther, A. B. et al. The Model of Emissions of Gases and Aerosols from Nature version 2.1 (MEGAN2.1): an extended and updated framework for modeling biogenic emissions. *Geosci. Model Dev.* **5**, 1471–1492 (2012).
- Fairlie, T., Jacob, D. & Park, R. The impact of transpacific transport of mineral dust in the United States. *Atmos. Environ.* **41**, 1251–1266 (2007).
- Hanson, D. R., Burkholder, J. B., Howard, C. J. & Ravishankara, A. R. Measurement of OH and HO<sub>2</sub> radical uptake coefficients on water and sulfuric-acid surfaces. *J. Phys. Chem.* **96**, 4979–4985 (1992).
- Gershenzon, Y. M., Grigorieva, V. M., Ivanov, A. V. & Remorov, R. G. O<sub>3</sub> and OH sensitivity to heterogeneous sinks of HO<sub>2</sub> and CH<sub>3</sub>O<sub>2</sub> on aerosol particles. *Faraday Discuss.* **100**, 83–100 (1995).
- Matthews, P. S. J., Baeza-Romero, M. T., Whalley, L. K. & Heard, D. E. Uptake of HO<sub>2</sub> radicals onto Arizona test dust particles using an aerosol flow tube. *Atmos. Chem. Phys.* **14**, 7397–7408 (2014).
- Taketani, F. et al. Measurement of overall uptake coefficients for HO<sub>2</sub> radicals by aerosol particles sampled from ambient air at mts. Tai and Mang (China). *Atmos. Chem. Phys.* **12**, 11907–11916 (2012).
- Zhou, J., Murano, K., Kohno, N., Sakamoto, Y. & Kajii, Y. Real-time quantification of the total HO<sub>2</sub> reactivity of ambient air and HO<sub>2</sub> uptake kinetics onto ambient aerosols in Kyoto (Japan). *Atmos. Environ.* **223**, 117189 (2020).
- Lahey, P. S. J., George, I. J., Baeza-Romero, M. T., Whalley, L. K. & Heard, D. E. Organics substantially reduce HO<sub>2</sub> uptake onto aerosols containing transition metal ions. *J. Phys. Chem. A* **120**, 1421–1430 (2016).
- Thornton, J. & Abbatt, J. P. D. Measurements of HO<sub>2</sub> uptake to aqueous aerosol: mass accommodation coefficients and net reactive loss. *J. Geophys. Res. Atmos.* **110**, D08309 (2005).
- Taketani, F., Kanaya, Y. & Akimoto, H. Kinetics of heterogeneous reactions of HO<sub>2</sub> radical at ambient concentration levels with (NH<sub>4</sub>)<sub>2</sub>(SO<sub>4</sub>) and NaCl aerosol particles. *J. Phys. Chem. A* **112**, 2370–2377 (2008).
- Schroeder, W. H., Dobson, M., Kane, D. M. & Johnson, N. D. Toxic trace elements associated with airborne particulate matter: a review. *J. Air Waste Manage. Assoc.* **37**, 1267–1285 (1987).
- Allen, A. G., Nemitz, E., Shi, J. P., Harrison, R. M. & Greenwood, J. C. Size distributions of trace metals in atmospheric aerosols in the United Kingdom. *Atmos. Environ.* **35**, 4581–4591 (2001).
- Ross, H. B. & Noone, K. J. A numerical investigation of the destruction of peroxy radical by Cu ion catalysed reactions on atmospheric particles. *J. Atmos. Chem.* **12**, 121–136 (1991).
- Mao, J., Fan, S., Jacob, D. J. & Travis, K. R. Radical loss in the atmosphere from Cu-Fe redox coupling in aerosols. *Atmos. Chem. Phys.* **13**, 509–519 (2013).

## Acknowledgements

This work was funded by the Natural Environment Research Council [NE/R017549/1]. We thank the UK National Centre for Atmospheric Science for funding and for use of the CEDA data repository. We thank the University of York for access to the Viking Cluster. We thank the GEOS-Chem community for developing the model over the past decades.

## Author contributions

P.D.I., M.J.E. and A.C.L. contributed to generating the ideas, methodology and writing. P.D.I. ran the simulations, adapted the model and generated the figures.

## Competing interests

The authors declare no competing interests.

## Additional information

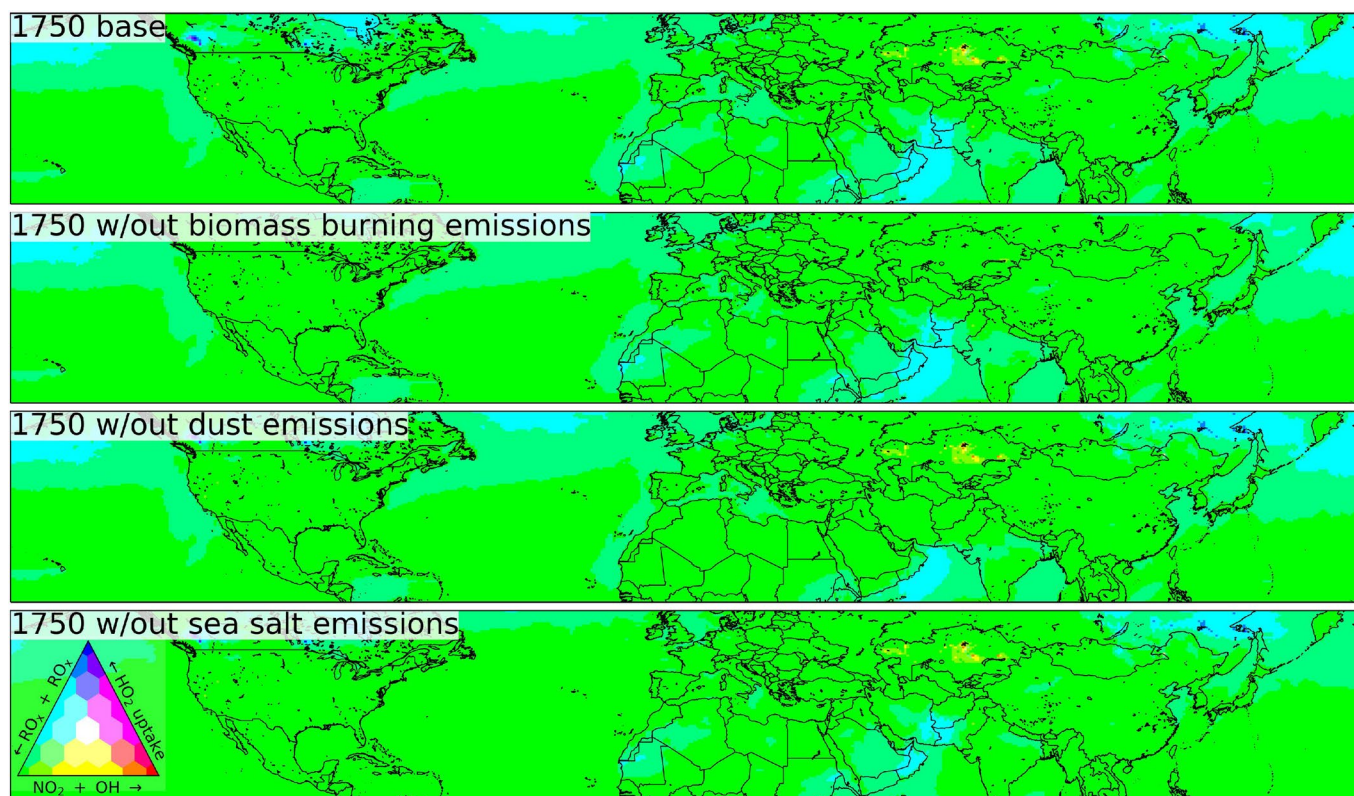
**Extended data** is available for this paper at <https://doi.org/10.1038/s41561-022-00972-9>.

**Supplementary information** The online version contains supplementary material available at <https://doi.org/10.1038/s41561-022-00972-9>.

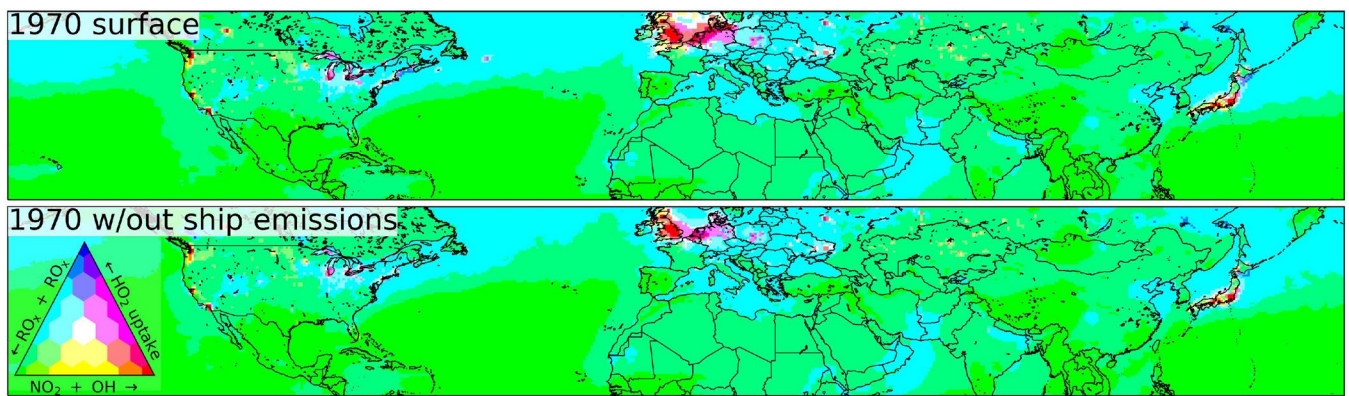
**Correspondence and requests for materials** should be addressed to Mathew J. Evans.

**Peer review information** *Nature Geoscience* thanks Keding Lu and the other, anonymous, reviewer(s) for their contribution to the peer review of this work. Primary Handling Editors: Xujia Jiang and Thomas Richardson, in collaboration with the *Nature Geoscience* team

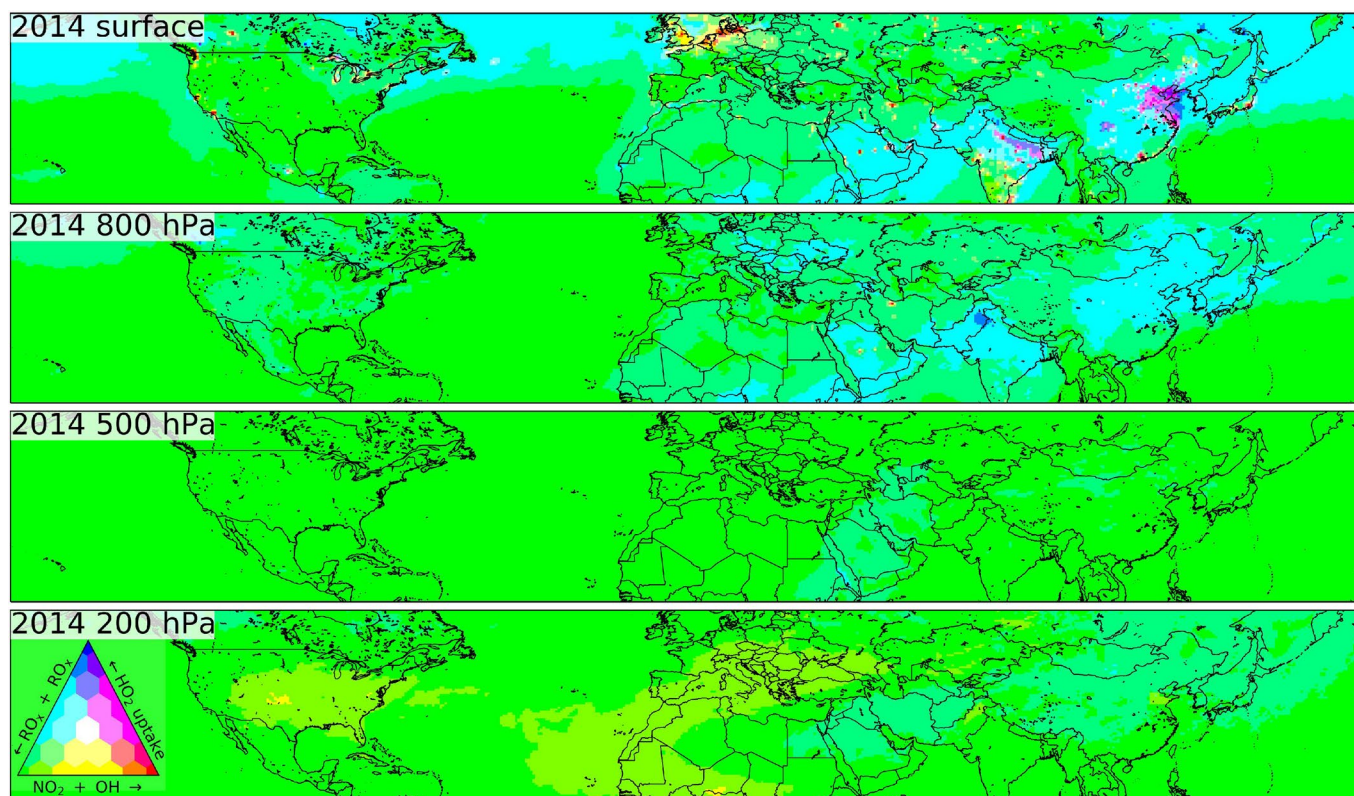
**Reprints and permissions information** is available at [www.nature.com/reprints](http://www.nature.com/reprints).



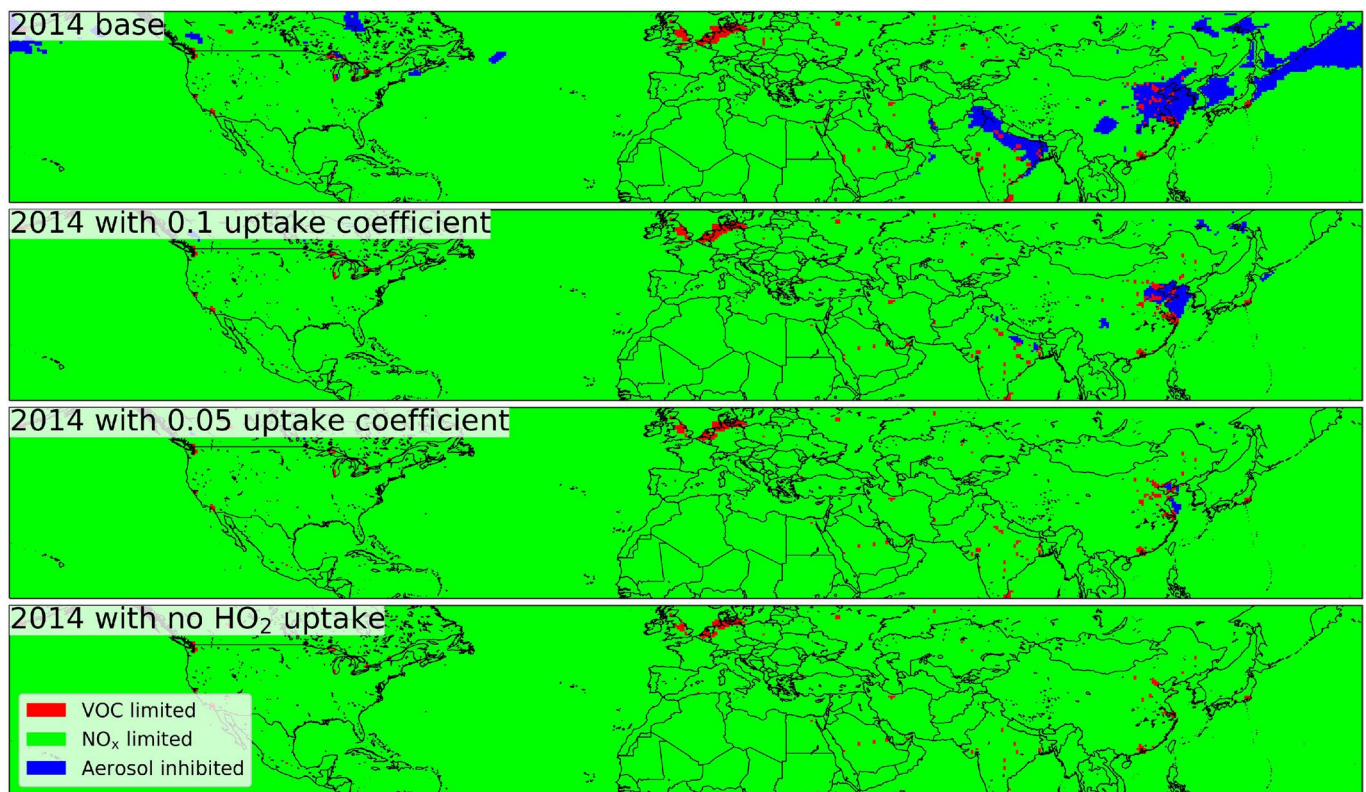
**Extended Data Fig. 1 | Map of the fractional contribution of radical loss pathways under different 1750 emission scenarios.** Average simulated July noon-time fraction of radical termination at the surface that occurs through the  $\text{OH} + \text{NO}_2$ , peroxy radical self-reactions and aerosol uptake of  $\text{HO}_2$  for 1750 in the base model, without any biomass burning, without any desert dust emissions, and without any sea salt emissions.



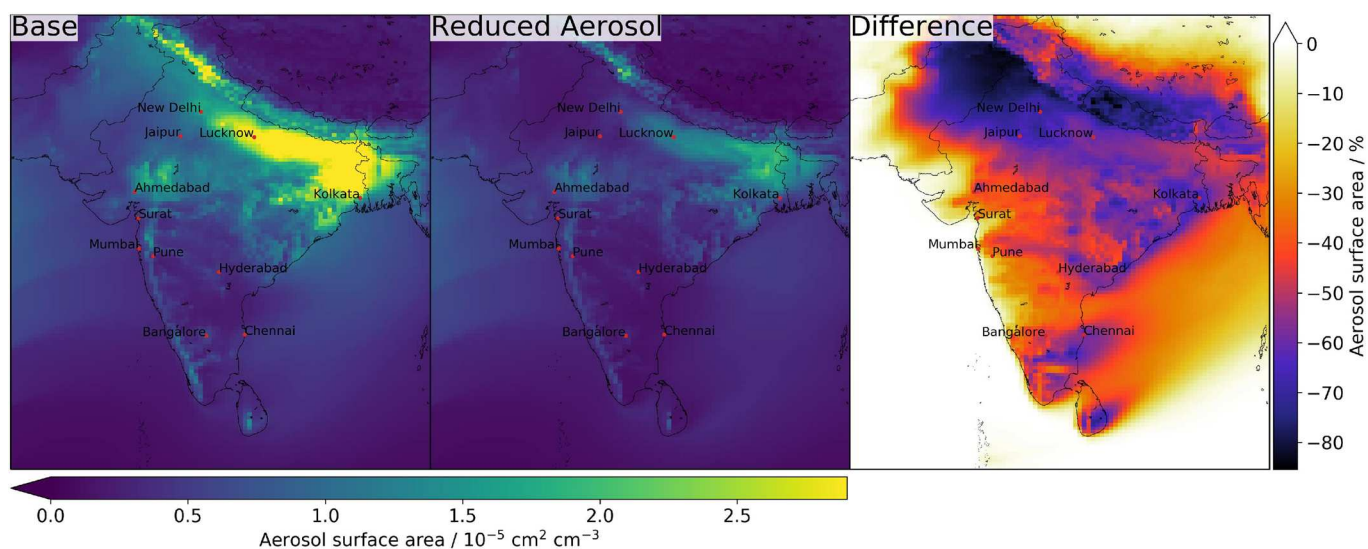
**Extended Data Fig. 2 | Map of the fractional contribution of radical loss pathways with and without shipping emissions in 1970.** Average simulated July noon-time fraction of radical termination at the surface that occurs through the OH + NO<sub>2</sub>, peroxy radical self-reactions and aerosol uptake of HO<sub>2</sub> for 1970 in the model with and without shipping emissions.



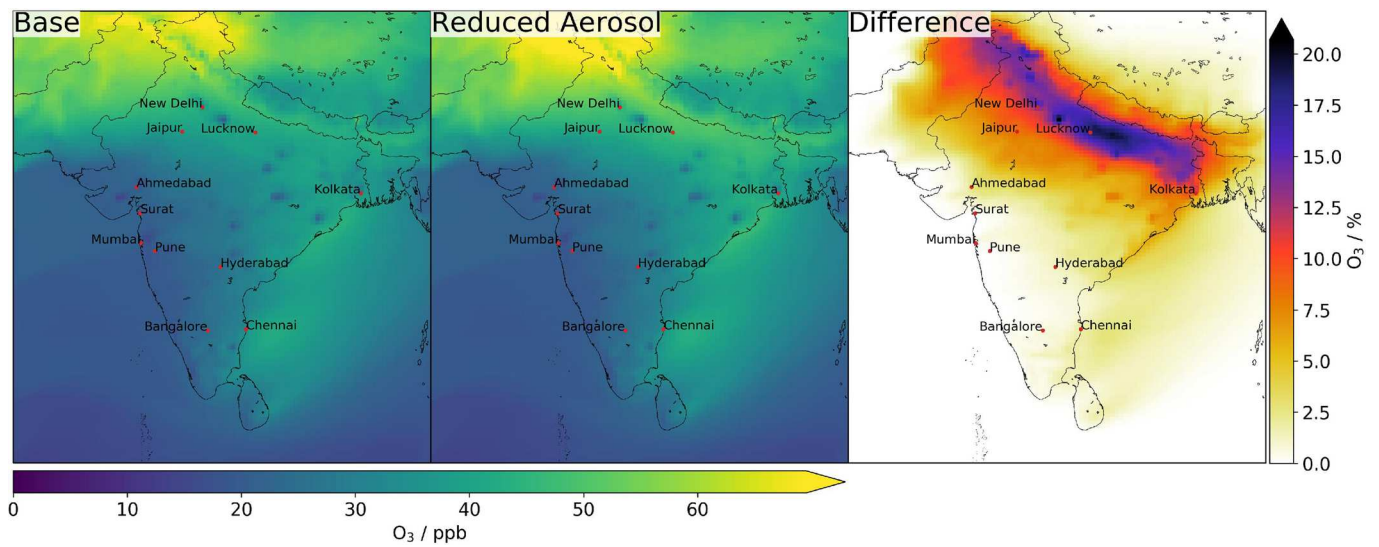
**Extended Data Fig. 3 | Fractional contribution of radical loss pathways in 2014 at different altitudes.** Average simulated July noon-time fraction of radical termination that occurs through the  $\text{OH} + \text{NO}_2$ , peroxy radical self-reactions and aerosol uptake of  $\text{HO}_2$  at the surface, 800 hPa, 500 hPa and 200 hPa.



**Extended Data Fig. 4 |** Map of the fractional contribution of radical loss pathways in 2014 with different  $\text{HO}_2$  uptake coefficients. Average simulated July noon-time photochemical regime in 2014 with  $\gamma_{\text{HO}_2}$  of 0.2 (base), 0.1, 0.05 and 0.0.



**Extended Data Fig. 5 | Map of a 50% reduction in aerosol emissions in India.** July 2014 mean surface aerosol surface area density over India in a base simulation and in a simulation with a 50% reduction in emission of aerosol precursors (anthropogenic  $\text{SO}_2$ , black carbon, organic carbon, dust, and all biomass burning emissions).



**Extended Data Fig. 6 | Map of the ozone change with a 50% reduction in aerosol emissions in India.** July 2014 mean O<sub>3</sub> mixing ratios over India in a base simulation and in a simulation with a 50% reduction in emission of aerosol precursors (anthropogenic SO<sub>2</sub>, black carbon, organic carbon, dust, and all biomass burning emissions).